Thickness Profiles of Retinal Layers by Optical Coherence Tomography Image Segmentation

AHMET MURAT BAGCI, MAHNAZ SHAHIDI, RASHID ANSARI, MICHAEL BLAIR, NORMAN PAUL BLAIR, AND RUTH ZELKHA

• PURPOSE: To report an image segmentation algorithm that was developed to provide quantitative thickness measurement of six retinal layers in optical coherence tomography (OCT) images.

• DESIGN: Prospective cross-sectional study.

• METHODS: Imaging was performed with time- and spectral-domain OCT instruments in 15 and 10 normal healthy subjects, respectively. A dedicated software algorithm was developed for boundary detection based on a 2-dimensional edge detection scheme, enhancing edges along the retinal depth while suppressing speckle noise. Automated boundary detection and quantitative thickness measurements derived by the algorithm were compared with measurements obtained from boundaries manually marked by three observers. Thickness profiles for six retinal layers were generated in normal subjects.

• RESULTS: The algorithm identified seven boundaries and measured thickness of six retinal layers: nerve fiber layer, inner plexiform layer and ganglion cell layer, inner nuclear layer, outer plexiform layer, outer nuclear layer and photoreceptor inner segments (ONL+PIS), and photoreceptor outer segments (POS). The root mean squared error between the manual and automatic boundary detection ranged between 4 and 9 μm. The mean absolute values of differences between automated and manual thickness measurements were between 3 and 4 μm, and comparable to interobserver differences. Inner retinal thickness profiles demonstrated minimum thickness at the fovea, corresponding to normal anatomy. The OPL and ONL+PIS thickness profiles respectively displayed a minimum and maximum thickness at the fovea. The POS thickness profile was relatively constant along the scan through the fovea.

• CONCLUSIONS: The application of this image segmentation technique is promising for investigating thickness changes of retinal layers attributable to disease progression and therapeutic intervention. (Am J Ophthalmol 2008;146:679–687. © 2008 by Elsevier Inc. All rights reserved.)

Accepted for publication Jun 10, 2008.

From the Departments of Electrical and Computer Engineering (A.M.B., R.A.); and Ophthalmology and Visual Sciences (M.S., M.B., N.P.B., R.Z.), University of Illinois at Chicago, Chicago, Illinois.

Inquiries to Mahnaz Shahidi, Department of Ophthalmology and Visual Sciences, University of Illinois at Chicago, 1855 West Taylor Street, Chicago, IL 60612; e-mail: mahnshah@uic.edu

OPTICAL COHERENCE TOMOGRAPHY (OCT) IS AN imaging modality that provides cross-sectional images of the retina. The commercially available time-domain (TD) OCT instrument provides software for measurement of total retinal thickness, therefore limiting information on the thickness of retinal layers. Thickness measurement of retinal layers is important as it provides useful information for detecting pathologic changes and diagnosing retinal diseases.

Recently, various approaches have been described for retinal thickness measurements from OCT images. Ishikawa and associates have described an approach to segment and extract thickness of retinal layers from Stratus and ultra-high-resolution OCT images.[1,2] However, thickness measurements of only four layer segments were derived. Koozekanani and associates described a method for extracting the upper and lower retinal boundaries on OCT images with the use of a Markov model.[3] While this algorithm has shown to be robust, it is limited to detection of only two boundaries. Recently, a method based on an extension of the Markov model was reported for analysis of optic nerve head geometry.[4] Determination of retinal nerve fiber layer thickness based on a deformable spline algorithm has also been reported.[5] This algorithm was developed for tracking nerve fiber layer (NFL) in OCT movies and may be inadequate for detecting multiple layers with varying contrast and noise.

Several factors reduce the sharpness of retinal layer boundaries in OCT images and prove challenging for continuous edge detection and accurate retinal layer identification. We have developed a new algorithm to automatically detect retinal layer boundaries and measure the thickness of six layers within the retinal tissue. Our method has advantages over previously reported methods because it utilizes a customized filter for edge enhancement and a gray-level mapping technique that overcomes uneven tissue reflectivity and intersubject variations. In this article, we report the application of this method to time- and spectral-domain (SD) OCT images, comparison of automated and manual segmentation, and a normal baseline for thickness of retinal layers.

METHODS

• SUBJECTS: OCT imaging (Stratus time-domain OCT) was performed in one eye of 15 normal subjects, 10 women

0002-9394/08/$34.00
doi:10.1016/j.ajo.2008.06.010

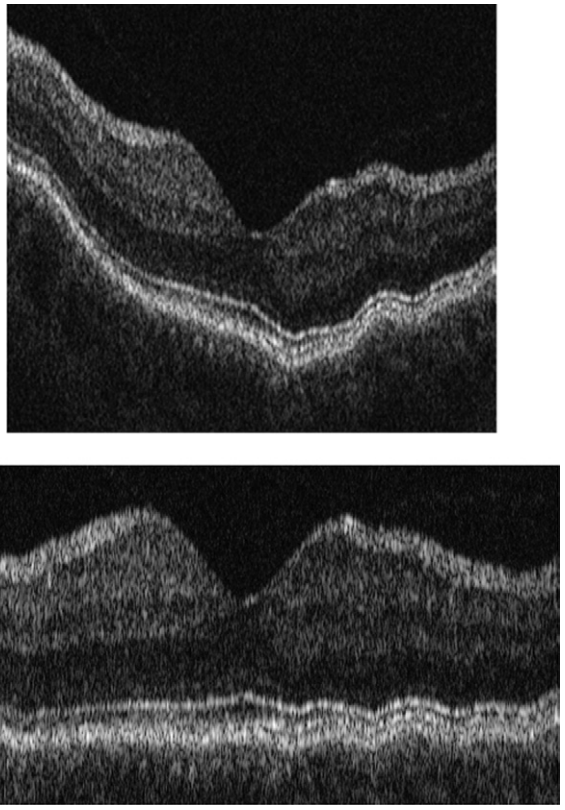

FIGURE 1. Retinal layer segmentation step of A-scan alignment applied to a typical time-domain optical coherence tomography (TD OCT) image. (Top) Example of a TD OCT image obtained in one of the subjects in the study. (Bottom) OCT image after alignment of A-scans.

and five men, six left and nine right eyes. The subjects' ages ranged between 42 and 78 years, with an average of 57 ± 11 years (mean ± standard deviation [SD]). OCT imaging (RTVue spectral-domain OCT) was performed in one eye of 11 normal subjects, 10 women and one man, six left and five right eyes. The subjects' ages ranged between 45 and 75 years, with an average of 56 ± 7 years (mean ± SD). Three images were obtained in each eye of 10 subjects. The subjects had ophthalmoscopic examination and no abnormalities were identified.

• **IMAGE ACQUISITION:** TD OCT imaging was performed using a Stratus OCT commercial instrument (Carl Zeiss Meditec, Dublin, California, USA). Six radial OCT scans, each 6 mm in length, were acquired. Each radial OCT scan was 1024 pixels (2 mm) in depth and 512 pixels (6 mm) in length and thus had a depth resolution of 2 μm/pixel and spatial resolution of 12 μm/pixel. The vertical (scan one of six) and horizontal (scan four of six) OCT scans were analyzed. The raw grayscale OCT images were exported for analysis. An example of an OCT image is shown in Figure 1. Each cell layer within the retina tissue displays different reflectance properties and produces peaks on a line profile across the retinal depth.

Spectral-domain OCT imaging was performed using an RTVue100 OCT commercial instrument (Optovue, Fremont, California, USA). Thirty-four raster OCT scans (MM5 protocol) were acquired and exported in TIF format. The vertical scan (scan 17) obtained in 10 subjects was analyzed for deriving thickness profiles. Fourteen OCT scans in the foveal and parafoveal areas of one subject were selected for comparing automated and manual boundary detection. The three horizontal scans (scans three, six, and nine of 34) and three vertical scans (scans 14, 17, and 20 of 34) were 640 pixels (2 mm) in depth and 669 pixels (5 mm) in length. The four horizontal scans (scans 23, 25, 26, and 28 of 34) and four vertical scans (scans 29, 31, 32, and 34 of 34) were 640 pixels (2 mm) in depth and 401 pixels (3 mm) in length. The scans had a depth resolution of 3 μm/pixel and spatial resolution of 7.5 μm/pixel.

• **IMAGE ANALYSIS:** A dedicated software program was developed in Matlab (The Mathworks Inc, Natick, Massachusetts, USA) for automated image analysis, without manual processing. The image analysis algorithm[6] segmented the OCT image by the following steps: 1) alignment of A-scans; 2) gray-level mapping; 3) directional filtering; 4) edge detection; and 5) model-based decision making.

Alignment of A-scans. Common reference points in each A-scan were identified using a two-pass edge detection algorithm[6] and A-scans were shifted so that each reference point was at the same level as the neighboring column. At each pass, the images were smoothed using a Gaussian filter, the derivative of the image in the vertical direction (depth) was calculated, single pixel edges were obtained using nonmaximum suppression, and broken edges were eliminated by hysteresis thresholding, similar to Canny edge detection.[7] Gaussian filtering with a larger support provided the two most prominent edges corresponding to the inner limiting membrane (ILM) and retinal pigment epithelium (RPE). The image was aligned according to the RPE boundary, by shifting each A-scan vertically. Because of heavy blurring to suppress noise, these locations were approximate. Therefore, a second pass was performed with a Gaussian filter with a smaller support for more accurate alignment. Only edges that coincided with the first pass were chosen and A-scans were shifted to their final position. The blurring operations were only used to locate the RPE boundary initially, and did not change the pixel intensity values. The image shown in Figure 1, Top was aligned using this algorithm and the output is shown in Figure 1, Bottom. The algorithm then aligns the A-scans according to a finer boundary, namely, the junction between photoreceptor inner and outer segments (IS/OS). Alignment of A-scans was needed for TD OCT images, attributable to eye motion artifacts because of slower image acquisition time, as compared with SD OCT (see Figure 4, Top row). This alignment step may be eliminated for SD OCT images, since it did not significantly improve images.

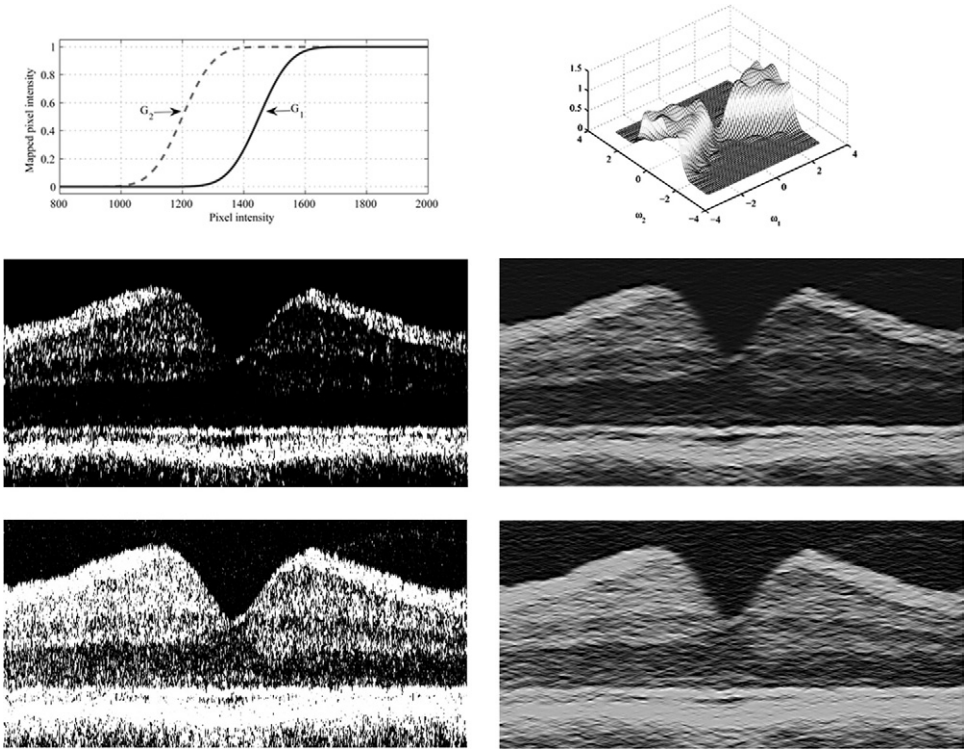

FIGURE 2. Retinal layer segmentation steps of gray-level mapping and directional filtering applied to a typical TD OCT image. (Top left) Two functions (G_1 and G_2) used for gray-level mapping of the image in Figure 1. (Second row, left) Image after gray-level mapping with G_1, depicts boundaries between nerve fiber layer (NFL) and inner plexiform layer and ganglion cell layer (IPL+GCL), the junction between photoreceptor inner and outer segments (IS/OS) and retinal pigment epithelium (RPE). (Third row, left) Image after gray-level mapping with G_2, depicts the remaining boundaries. (Top right) Frequency response of a wedge-shaped 2-dimensional directional filter. (Second row, right) Image displayed in second row, left after directional filtering. (Third row, right) Image displayed in third row, left, after directional filtering. The IS/OS interface appears flat, because of the initial alignment step.

Gray-Level Mapping. In OCT images, the region between the RPE boundary and ILM contains primarily three stratified brightness levels and six layers. The transitions between these layers produce edges with different strengths. For example, a typical transition from NFL to inner plexiform layer and ganglion cell layer (IPL+GCL) represents an approximate change in gray-level value from 1800 to 1100 (12-bit data), whereas a transition from outer plexiform layer (OPL) to outer nuclear layer (ONL) translates to a change in approximate gray-level value from 1200 to 900. The second transition produces a weaker edge. To strengthen the weak edges, an adaptive gray-level mapping using two mapping functions was performed.[6] The parameters that defined the mapping were decided adaptively for each OCT image using the expectation maximization (EM) algorithm.[8] The two mapping functions, G1 and G2, obtained for the image in Figure 1 are plotted in Figure 2, Top right. The boundaries between NFL and IPL+GCL, IS/OS interface, and RPE layer were determined with G1 (Figure 2, Second row, left), while the remaining boundaries were determined with G2 (Figure 2, Third row, left). The IS/OS interface appears flat, because of the initial alignment step.

Directional Filtering. To overcome edge blurring, a 2-dimensional filter with a wedge-shaped pass band was employed. The design of the directional filter banks was based on our previously published method.[9] This filter suppressed the speckle noise that produces high-frequency variances in horizontal direction, while keeping the detail in vertical direction, which contained the boundary information. The filter preserved edges lying within ±45 degrees of the horizontal axis, which emphasizes the importance of aligning columns so that boundaries had a slope close to 0 degrees. The frequency response of the filter is shown in Figure 2, Top left. Images following gray-level mapping in Figure 2, Left panels were processed by directional filtering algorithm and displayed in Figure 2, Right panels.

Edge Detection. An edge detection kernel based on the first derivative of Gaussian in the vertical direction was used for obtaining candidate contours for boundaries.[6] The edge detection kernel was applied twice. First, the boundaries between each pair of adjacent bright and dark regions, with bright on the anterior, were extracted. In the second pass, boundaries between each pair of adjacent bright and dark regions, with dark on

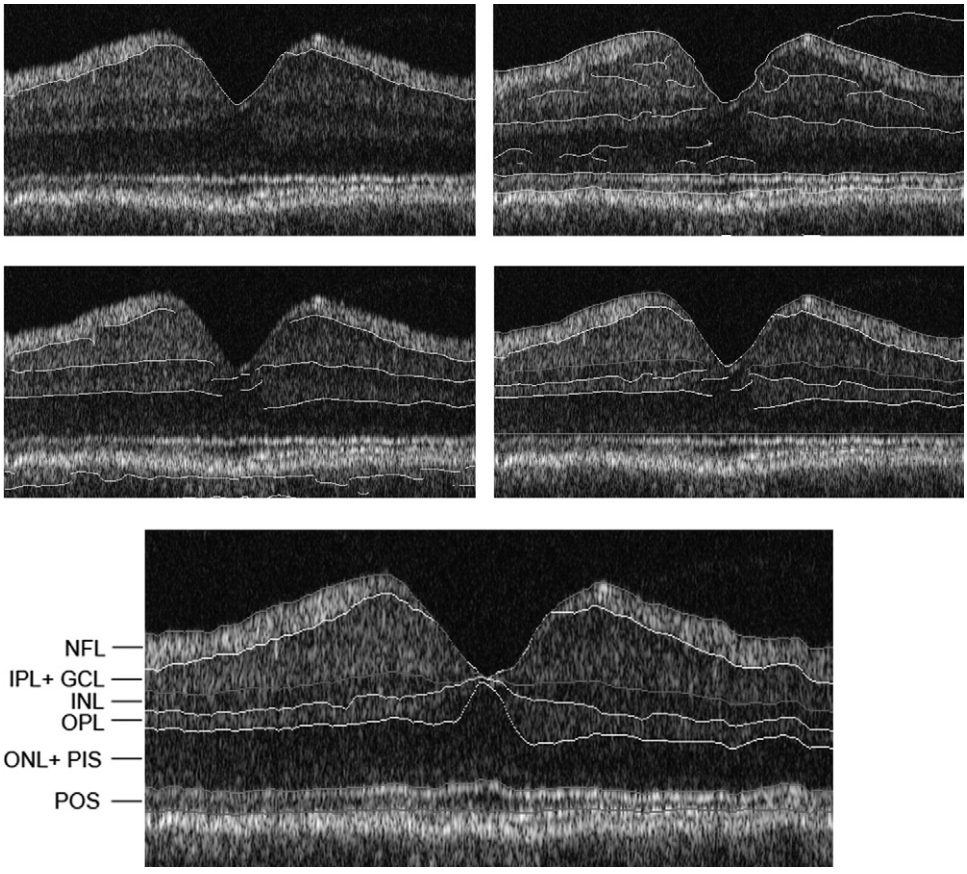

FIGURE 3. Retinal layer segmentation step of edge detection applied to a typical TD OCT image. (Top left) Edge detection following processing steps displayed in Figure 2 with boundary contour overlaid on the original image. Edge detection following processing steps displayed in Figure 2 with boundary contours overlaid on the original image for (Second row, left) bright-to-dark transitions and (Top right) dark-to-bright transitions. (Second row, right) Boundary contours are displayed on the image following edge detection. (Bottom) Boundary lines were connected and the gaps filled according to the model; six retinal layers were segmented and labeled. After RPE boundary detection, the image was aligned again according to the RPE boundary to maintain the curvature of the IS/OS interface.

the anterior, were detected. The peak values were marked as edges, using nonmaximum suppression and hysteresis thresholding.[7] At the output of this step, major significant contour segments and their polarities were marked. The output consisted of contour segments with gaps. The contour segments derived by edge detection were overlaid on the original image. Figure 3, Top left displays NFL boundary, and Figure 3, Second row, left and Figure 3, Top right display bright-to-dark transitions and dark-to-bright transitions, respectively.

Model-Based Decision Making. The classification and labeling of edges and creation of continuous contours were performed in this step. The marking of ILM and RPE boundaries in the first step was found to be robust. These boundaries were therefore used to serve as reference points. A model that contained the approximate location of each boundary, along with the polarity of the edges that formed the boundary and relative location of boundaries with respect to each other, was used. For any column in the image (along the retinal depth), starting from the top (anterior) we expected to view boundaries between NFL, IPL+GCL, inner nuclear layer (INL), OPL, and ONL, which correspond to edges with the polarities (+1, +1, −1, +1), respectively. The set of contours obtained at the edge detection step that conformed to this particular order were labeled using this model. For a given column in the image, if the polarities of the contours did not match this order, they were not included in the selected contours. This selection was automatic. This method worked well for strong edges, but occasionally (13.3% of TD OCT and 6.6% of SD OCT images) some scattered light on the image was also marked as a boundary pixel. These false positives appeared as discontinuities along the boundary and were removed using a simple median filter. In the final step, the gaps along the boundary attributable to insufficient edge clues were filled. At this point, the model was fine-tuned using edge clues that were already labeled, and the gaps along the boundary were filled in according to the updated model. After RPE boundary detection, the image was aligned again according to the RPE boundary to maintain the curvature of

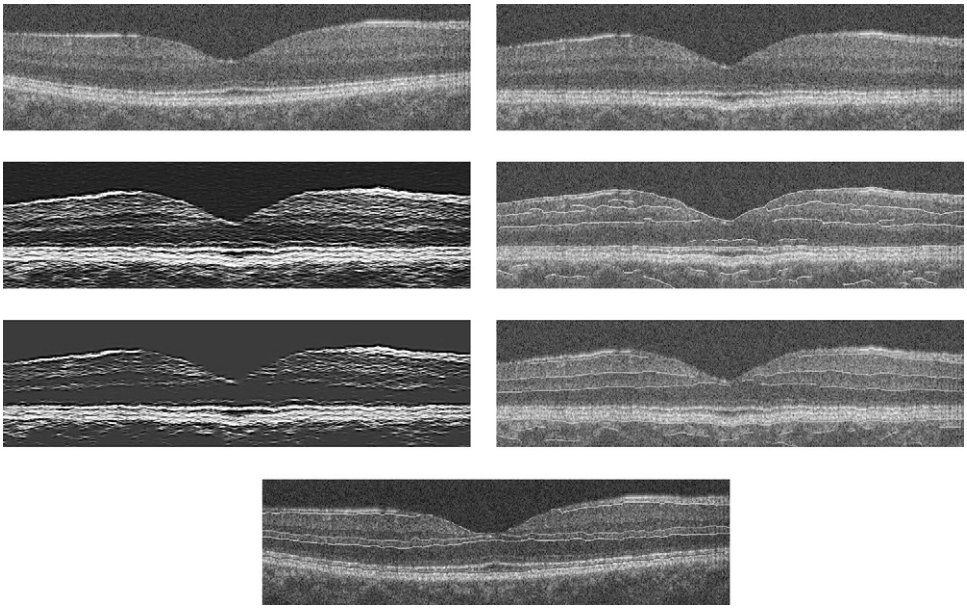

FIGURE 4. Retinal layer segmentation method applied to a typical spectral-domain OCT (SD OCT) image. (Top left) Example of a SD OCT image. (Top right) Image after A-scan alignment. (Second row, left) Image after gray-level mapping depicts boundaries between layers. (Second row, right) Image after edge detection for dark-to-bright transitions with boundary contours overlaid on the original image. (Third row, left) Image after gray-level mapping depicts NFL boundaries. (Third row, right) Image after edge detection for bright-to-dark transitions with boundary contours overlaid on the original image. (Bottom) Boundary lines were connected; six retinal layers were segmented.

the IS/OS interface. The connected contours are marked on the image in Figure 3, Bottom, which is the final output of the algorithm.

• **DATA ANALYSIS:** On each OCT image, seven boundaries were detected automatically by the segmentation algorithm. The same images were evaluated by three observers (M.B., R.Z., and N.B.) by manually drawing the boundaries. ImageJ software (NIH, Bethesda, Maryland, USA) was used to open the images, draw the boundaries, and then save the images. A Matlab program was written to compare images with automatically and manually drawn boundaries. The average root mean squared error (RMSE) values between the manually and automatically marked boundaries were calculated. Thickness profiles for each of the six retinal layers were calculated by first subtracting edge locations along the vertical direction (retinal depth) and then averaging thickness values along the horizontal direction, at an interval of every 200 μm. Intrasubject variability (reproducibility) was determined as the SD of three measurements in each subject, averaged over all subjects. Intersubject variability was determined as the mean SD of thickness measurements across all subjects.

TABLE 1. Automated and Manual Boundary Detection From Time-Domain Optical Coherence Tomography Images

Boundary	RMSE (μm) Mean ± Standard Deviation
1 = ILM	4.3 ± 0.9
2	8.2 ± 0.9
3	7.8 ± 0.3
4	7.7 ± 0.5
5	9.9 ± 0.7
6	3.5 ± 0.3
7 = RPE	7.8 ± 0.6

ILM = inner limiting membrane; RMSE = root mean squared error; RPE = retinal pigment epithelium.

Comparison of boundary detection between three observers (N.B., R.Z., and M.B.) and the automated algorithm. The RMSE was calculated and averaged over 15 time-domain optical coherence tomography images. The RMSE averaged over three observers is listed.

RESULTS

• **RETINAL LAYER SEGMENTATION:** The algorithm used the fact that the inner and OPLs appeared brighter than the inner and ONLs in the OCT image. In addition, NFL, RPE, and IS/OS appeared brighter than the rest of the layers. Overall, the algorithm identified the following six layers on the retinal image: NFL, IPL+GCL, INL, OPL, ONL+PIS, and photoreceptor outer segments (POS), as marked on the sample OCT scan shown in Figure 3, Bottom. The POS layer was bounded by IS/OS and RPE

TABLE 2. Automated and Manual Boundary Detection From Spectral-Domain Optical Coherence Tomography Images

Boundary	RMSE (μm) Mean ± Standard Deviation
1 = ILM	4.3 ± 0.8
2	5.7 ± 0.7
3	5.3 ± 0.5
4	6.1 ± 1.0
5	8.8 ± 1.2
6	4.3 ± 1.1
7 = RPE	5.5 ± 1.0

ILM = inner limiting membrane; RMSE = root mean squared error; RPE = retinal pigment epithelium.

Comparison of boundary detection between three observers (N.B., R.Z., and M.B.) and the automated algorithm. The RMSE was calculated and averaged over 14 spectral-domain optical coherence tomography images. The RMSE averaged over three observers is listed.

TABLE 3. Comparison of Automated and Manual Thickness Measurements

Layer	Thickness (μm) Mean ± Standard Deviation	
	Automated	Manual
NFL	31 ± 16	33 ± 15
IPL+GCL	68 ± 23	69 ± 22
INL	30 ± 8	27 ± 8
OPL	32 ± 9	33 ± 12
ONL+PIS	77 ± 20	77 ± 21
POS	37 ± 3	32 ± 3

NFL = nerve fiber layer; IPL+GCL = inner plexiform layer and ganglion cell layer; INL = inner nuclear layer; OPL = outer plexiform layer; ONL+PIS = outer nuclear layer and photoreceptor inner segments; POS = photoreceptor outer segments.

Mean and standard deviation of thickness profiles (averaged profiles from time-domain optical coherence tomography images of 15 normal subjects) for six retinal layers. Manual thickness measurements represent average values of three observers.

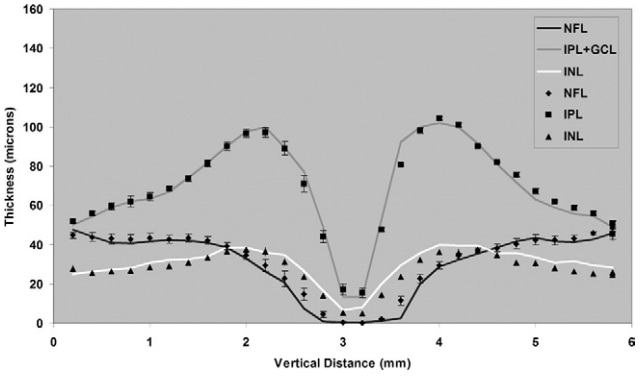

FIGURE 5. Comparison of automated and manual segmentation methods. Comparison of thickness profiles of inner retinal layers in 15 normal healthy subjects, derived from the automated algorithm (solid line) and manual segmentation; data averaged for three observers (symbols).

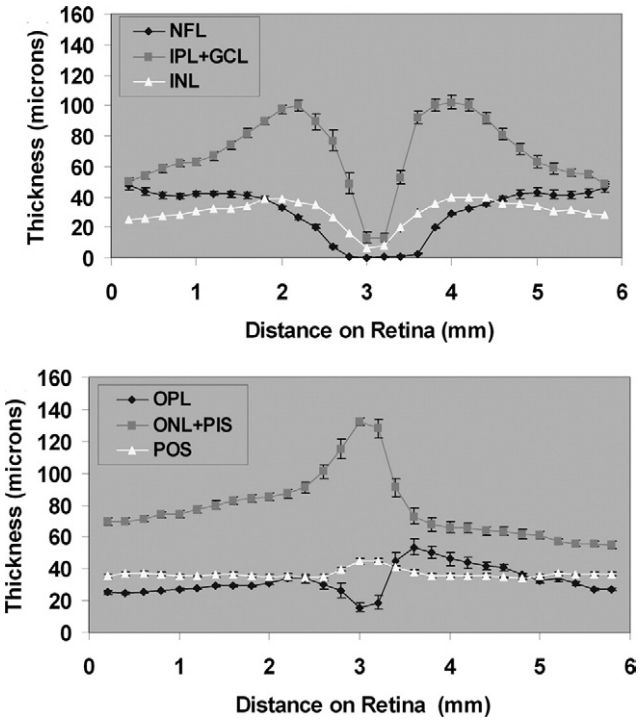

FIGURE 6. Thickness profiles in normal subjects from TD OCT images. Thickness profiles of inner (Top) and outer (Bottom) retinal layers measured from TD OCT image, averaged over 15 normal healthy subjects. Error bars represent standard error of the mean.

inner boundaries. The processing steps and layer segmentation for SD OCT images are depicted in Figure 4.

• **AUTOMATED AND MANUAL COMPARISON:** Seven boundaries were detected automatically by the segmentation algorithm in 15 TD OCT and 14 SD OCT images. The average RMSE between the manual and automatically marked boundaries on TD OCT images are presented in Table 1. The RMSE for detection of boundaries ranged between 3.5 and 9.9 μm (TD OCT). The average RMSE between the manual and automatically marked boundaries on SD OCT images are presented in Table 2. The RMSE for detection of boundaries ranged between 4.3 and 8.8 μm (SD OCT). For both the TD and SD OCT images, the least RMSE values were measured for detection of the ILM and IS/OS interfaces. The interface between the OPL and ONL had the largest RMSE value.

Thickness profiles of six retinal layers were derived based on automated and manual segmentation of 15 TD OCT

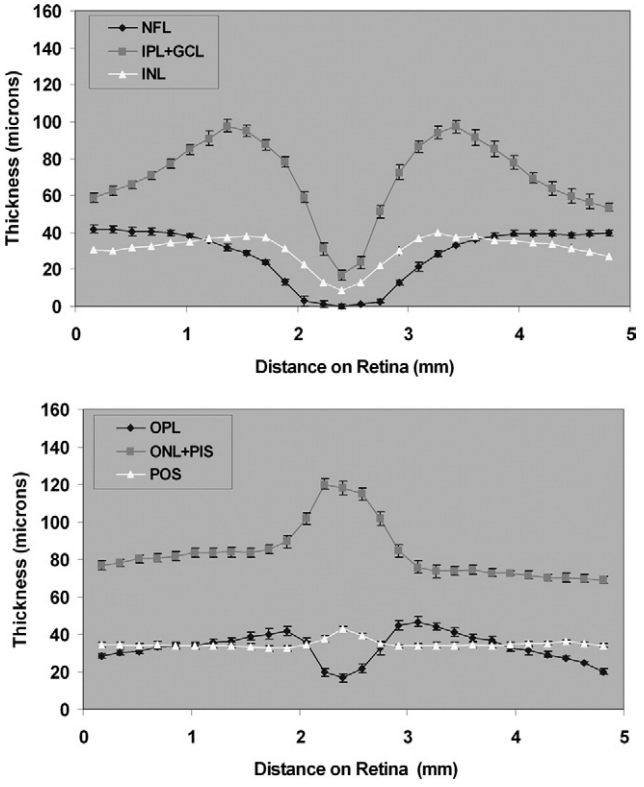

FIGURE 7. Thickness profiles in normal subjects from SD OCT images. Thickness profiles of inner (Top) and outer (Bottom) retinal layers measured from SD OCT image, averaged over 10 normal healthy subjects. Error bars represent standard error of the mean.

images (vertical scans). All six retinal layers were identified on each scan acquired in each of the 15 eyes. The thickness profiles derived from the automated algorithm (solid line) and manual segmentation, average data from three observers (symbols), are shown in Figure 5. The automated and manual thickness profiles appeared similar. NFL thickness showed an increase superior and inferior to the fovea, as expected. The IPL+GCL demonstrated a foveal depression, corresponding to normal anatomy. The mean absolute values of differences between the automated and manual thickness measurements were calculated. Combining measurements from six layers resulted in differences of 3.7 ± 2.0 μm (Auto-M.B.), 4.2 ± 1.7 μm (Auto-N.B.), and 3.0 ± 1.1 μm (Auto-R.Z.). The inter-observer differences for six layers were 3.4 ± 1.7 μm (M.B.-N.B.), 4.4 ± 2.1 μm (M.B.-R.Z.), and 3.8 ± 2.6 μm (N.B.-R.Z.). A comparison of thickness measurements for each layer by automated and manual (average measurements by three observers) segmentation is shown in Table 3. Mean and SD of thickness measurements by automated segmentations closely matched measurements obtained by manual segmentation. The absolute thickness difference ranged between 0 and 5 μm.

• **THICKNESS PROFILES IN NORMAL SUBJECTS:** Thickness profiles of six retinal layers measured along the 6-mm TD OCT vertical scan, averaged over 15 subjects, are shown in Figure 6. The thickness profiles of the inner retinal layers (NFL, IPL+GCL, INL) demonstrated a minimum thickness at the fovea. The maximum thickness of the NFL was 48 μm along the 6-mm scan. The thickness of the IPL+GCL ranged between 13 and 102 μm. The thickness of the INL ranged between 7 and 40 μm. The OPL thickness profile displayed a minimum thickness at the fovea and ranged between 16 and 54 μm along the 6-mm scan. The ONL+PIS thickness ranged between 55 and 132 μm and the profile displayed a maximum thickness at the fovea. The OPL was thicker and the ONL+PIS layer was thinner superior to the fovea as compared with a similar location inferior to the fovea. The POS thickness profile was relatively constant along the 6-mm scan through the fovea, ranging between 34 and 45 μm. Thickness profiles of six retinal layers measured along the 5-mm SD OCT vertical scan, averaged over 10 subjects, are shown in Figure 7. Thickness profiles obtained from SD OCT images displayed similar characteristics to those observed from analysis of TD OCT images. The mean intrasubject thickness measurement variability of NFL, IPL+GCL, INL, OPL, ONL+PIS, and POS was 3, 6, 4, 5, 4, and 2 μm, respectively. The mean intersubject thickness measurement variability of NFL, IPL+GCL, INL, OPL, ONL+PIS, and POS was 5, 10, 4, 6, 8, and 4 μm, respectively.

DISCUSSION

THE ABILITY TO MEASURE THICKNESS OF RETINAL LAYERS has potential value for early detection of pathologies and disease diagnosis. In this article, a new segmentation algorithm for automated detection of retinal layer boundaries and measurement of thickness of six layers within the retina tissue was presented. The results of automated segmentation corresponded well with normal retinal anatomy and with measurements obtained using manual segmentation by three observers. Thickness profiles for six retinal layers were established in normal healthy subjects at 200-μm intervals along a 6-mm vertical distance on the retina.

Retinal layer boundary detection by our automated algorithm was similar to manual outlining of the boundaries by human observers. The calculated RMSE was between 3 and 10 μm for detection of seven boundaries on both TD and SD OCT images. Thickness profiles derived by the automated algorithm were similar to profiles calculated from manual boundary detection. On average, the difference between automated and manual segmentation was ≤4.2 μm, and almost identical to the difference between manual measurements by three observers (≤4.4 μm).

Thickness profiles of inner retinal layers (NFL, IPL+GCL, INL) displayed a minimum at the center of

fovea, corresponding to normal anatomy. At the foveal center, thickness profiles of OPL and ONL+PIS displayed a minimum and maximum, respectively. Along the vertical scan, an asymmetry was observed in these layers. The OPL was thicker and the ONL+PIS was thinner superior to the fovea as compared with a similar location inferior to the fovea. The thickness asymmetry was observed on original TD and SD OCT vertical scans, even before image processing (Figure 1, Top), but not on horizontal scans. The observed asymmetry in reflectivity superior and inferior to the fovea was more prominent in TD OCT scans. The observed thickness asymmetry may be attributed to image acquisition artifacts or anatomy. Since most histologic studies are based on temporal-nasal sectioning of human retinas, a literature search yielded no reported information with regard to anatomic variations along the superior-inferior axis. Additional studies are needed to investigate the origin of the observed thickness asymmetry.

Previously reported edge detection algorithms were implemented on each image column individually to avoid complications attributable to misalignment of A-scans.[3] In contrast, we used the correlation between adjacent A-scans, which increases the effectiveness of edge detection. In previous studies, image noise was reduced by Gaussian filtering[10] and variants of median filtering.[2,3] While these methods are effective in suppressing noise, they also tend to reduce edge sharpness. To overcome edge blurring, we employed a 2-dimensional filter with a wedge-shaped pass band. This filter suppressed the speckle noise that produces high-frequency variances in horizontal direction, while keeping the detail in vertical direction, which contained the boundary information. Additionally, previous studies performed border detection initially on each A-scan individually, which limits the information from adjacent scans. In our algorithm, histogram equalization was performed on each A-scan to overcome uneven tissue reflectivity, which may also cause instability by amplifying the noise. Inhomogeneous retinal pathologies may cause local changes in reflectance from retinal layers, and thereby limit boundary detection. The influence of these changes on our segmentation algorithm and thickness measurements needs further investigation. Future studies are needed to establish the utility of this algorithm for images obtained in patients with retinal pathologies. An important application of this technique is for detection and monitoring of early and uniform changes in thickness of retinal layers. In more advanced disease, the normal stratification of the retinal layers may be lost. The influence of these changes on detection of retinal layer boundaries needs further investigation. In some instances, it may be necessary to measure thickness of combined layers.

Since our algorithm determines thickness of six retinal layers, the thickness sum of layers had to be calculated to compare results with previously reported techniques that measure thickness of up to four layers. The inner retina thickness measurements reported previously[10] were 170 ± 39 μm and were consistent with measurements (161 ± 33 μm) obtained by our algorithm as sum thickness of NFL+IPL+GCL+INL+OPL. The outer retinal thickness measurements reported previously[10] were 78 ± 10 μm, similar to thickness measurements of 77 ± 11 μm derived for ONL+PIS by our algorithm. Thickness measurements of NFL and inner retina complex (IRC) were reported to be 28.4 ± 4.7 μm and 90.7 ± 4.2 μm (reference 2). These values are consistent with thickness measurements of NFL (31 ± 6 μm) and IPL+GCL+INL (98 ± 19 μm). However, the previously reported[2] thickness measurement of OPL (51.0 ± 4.2 μm) based on low-resolution TD images (128 A-scans) are larger than thickness measurements of OPL (32 ± 8 μm) in the current study based on high-resolution TD images (512 A-scans). This discrepancy may be attributed to the difference in OCT image resolution. Outer retina complex (ORC) thickness has been reported to be 93.8 ± 7.3 μm (reference 2) and 91.1 ± 7.9 μm (reference 1), which is lower than the thickness of ONL+PIS+POS, measured along the 6-mm scan to be in the range of 91 and 177 μm (114 ± 16 μm) by our algorithm. From histologic studies,[11] POS has been measured to be 20 to 30 μm, which is consistent with measurements of 37 ± 4 μm (TD OCT) and 35 ± 4 μm (SD OCT) in our study. The observed differences in the ORC thickness derived by our algorithm and a previously reported algorithm[2] may be attributable to a dissimilarity in localization of IS/OS interface and RPE. Additionally, in the current study results were obtained from a single OCT image, while thickness was averaged over six radial OCT images and incorporated interpolated point values, in the previous study.

In summary, our algorithm has advantages over previously reported methods because it uses a customized filter to enhance edges along the retinal depth while suppressing speckle noise and a gray-level mapping technique to overcome uneven tissue reflectivity and variance across subjects. The application of this technique is promising for investigating thickness changes of retinal layers attributable to disease.

THIS STUDY WAS SUPPORTED BY THE DEPARTMENT OF VETERANS AFFAIRS, WASHINGTON, DC, NIH GRANTS EY14275 AND EY01792, Bethesda, Maryland; and an Unrestricted Departmental Grant from Research to Prevent Blindness Inc, New York, New York. The authors indicate no financial conflict of interest. Involved in design and conduct of study (M.S., A.B., R.A.); collection, management, analysis, and interpretation of data (N.B., M.B., R.Z., A.B., R.A., M.S.); and preparation, review, or approval of the manuscript (M.S., N.B., M.B., A.B., R.A.). The study was approved by the University of Illinois at Chicago Institutional Review Board, and proper informed consent was obtained according to the tenets of the Declaration of Helsinki participation in the research and HIPAA compliance was obtained.

REFERENCES

1. Chan A, Duker JS, Ishikawa H, Ko TH, Schuman JS, Fujimoto JG. Quantification of photoreceptor layer thickness in normal eyes using optical coherence tomography. Retina 2006;26:655–660.
2. Ishikawa H, Stein DM, Wollstein G, Beaton S, Fujimoto JG, Schuman JS. Macular segmentation with optical coherence tomography. Invest Ophthalmol Vis Sci 2005; 46:2012–2017.
3. Koozekanani D, Boyer K, Roberts C. Retinal thickness measurements from optical coherence tomography using a Markov boundary model. IEEE Trans Med Imaging 2001;20: 900–916.
4. Boyer KL, Herzog A, Roberts C. Automatic recovery of the optic nerve head geometry in optical coherence tomography. IEEE Trans Med Imaging 2006;25:553–570.
5. Mujat M, Chan R, Cense B, et al. Retinal nerve fiber layer thickness map determined from optical coherence tomography images. Optics Express 2005;13:9480–9491.
6. Bagci A, Ansari R, Shahidi M. A method for detection of retinal layers by optical coherence tomography image segmentation [conference proceedings]. IEEE/NLM Proc LISSA 2007;144–147.
7. Canny J. A computational approach to edge detection. IEEE Trans Pattern Anal Mach Intell 1986;8:679–698.
8. Dempster A, Laird N, Rubin D. Maximum likelihood from incomplete data via the EM algorithm. J R Stat Soc 1977; 39:1–38.
9. Bagci A, Ansari R, Reynold W. Low-complexity implementation of non-subsampled directional filter banks using polyphase representations and generalized separable processing [conference proceedings]. IEEE Proc EIT 2007:422–427.
10. Shahidi M, Wang Z, Zelkha R. Quantitative thickness measurement of retinal layers imaged by optical coherence tomography. Am J Ophthalmol 2005;139:1056–1061.
11. Hoang QV, Linsenmeier RA, Chung CK, Curcio CA. Photoreceptor inner segments in monkey and human retina: mitochondrial density, optics, and regional variation. Vis Neurosci 2002;19:395–407.

Biosketch

Ahmet M. Bagci, MS, received his BS degree in 1999 and MS degree in 2001 in Electrical Engineering from Bilkent University, Ankara, Turkey. Currently, he is a doctoral candidate at the Electrical and Computer Engineering Department at the University of Illinois at Chicago, Chicago, Illinois. Mr Bagci's area of research is signal and image processing, development of algorithms and methods for segmentation of medical images.